

Fig. S1. Innervation of the dorsal part of the diaphragm is also impaired in *Clpr-59*^{-/-} embryos from E15.5 to E18.5. Whole-mount histochemistry was performed on diaphragms using anti-peripherin to label embryonic nerve intermediate filaments and α -bungarotoxin to label nAChRs before macroscopic imaging (orientation of the diaphragm: D, dorsal; V, ventral; R, right; L, left). (A) The innervation patterns of the diaphragms are similar for control and for CLIPR-59-deficient embryos until E15.5, as the dorsal and ventral primary branches of the phrenic nerve reach both muscle extremities. (B) At E18.5, both ventral and dorsal branches of phrenic nerves do not reach the most distal part of the mutant diaphragm. (C) In the magnification of the dorsal region of the diaphragm muscle, the innervation pattern in the mutant becomes incomplete from E15.5 until E18.5. Scale bar: 500 μ m.

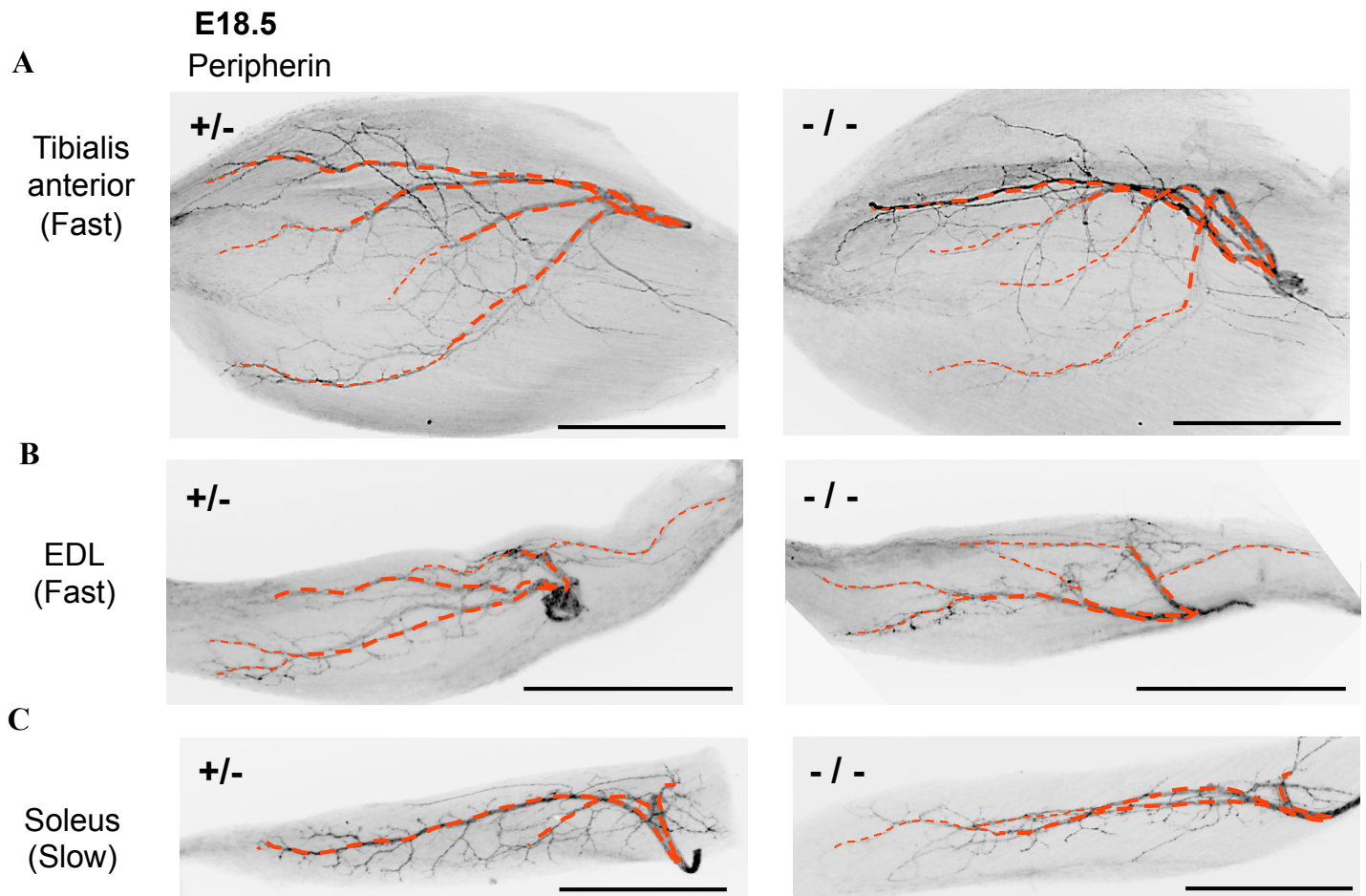


Fig. S2. Innervation defects in hindlimb muscles are less extended than in diaphragm of *Clpr-59*^{-/-} embryos at E18.5. Whole-mount histochemistry was performed on dissected hindlimb muscles using anti-peripherin to label embryonic nerve intermediate filaments before macroscopic imaging. To facilitate the visualization and comparison of the innervation, the nerve trunk is highlighted by a broken red line. (A,B) In E18.5 mutant embryos, the innervation pattern is moderately altered in two fast-twitch muscles, (A) the tibialis anterior and (B) the extensor digitorum longus (EDL). (C) In the slow-twitch muscle soleus, only slight innervation defects can be detected in the mutant at E18.5. Scale bar: 500 μ m.

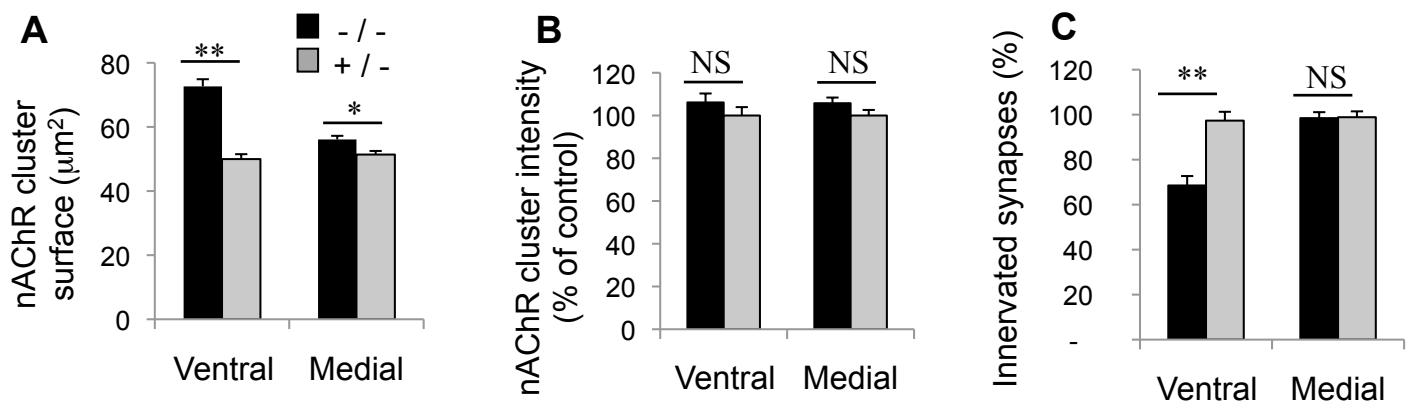


Fig. S3. Post-synaptic nAChRs are slightly less clustered in the denervated part of the mutant diaphragms at E18.5. Post-synaptic nAChRs were labeled with α -bungarotoxin in whole-mount diaphragm preparations and then imaged by confocal microscopy. (A-C) Measurement of (A) nAChR cluster surface, (B) α -Bungarotoxin fluorescence signal intensity and (C) percentage of innervated synapses were performed in the ventral and medial parts of the diaphragm at E18.5. Data are mean \pm s.e.m. * P <0.05; ** P <0.001; Mann-Whitney U test. NS, non significant.

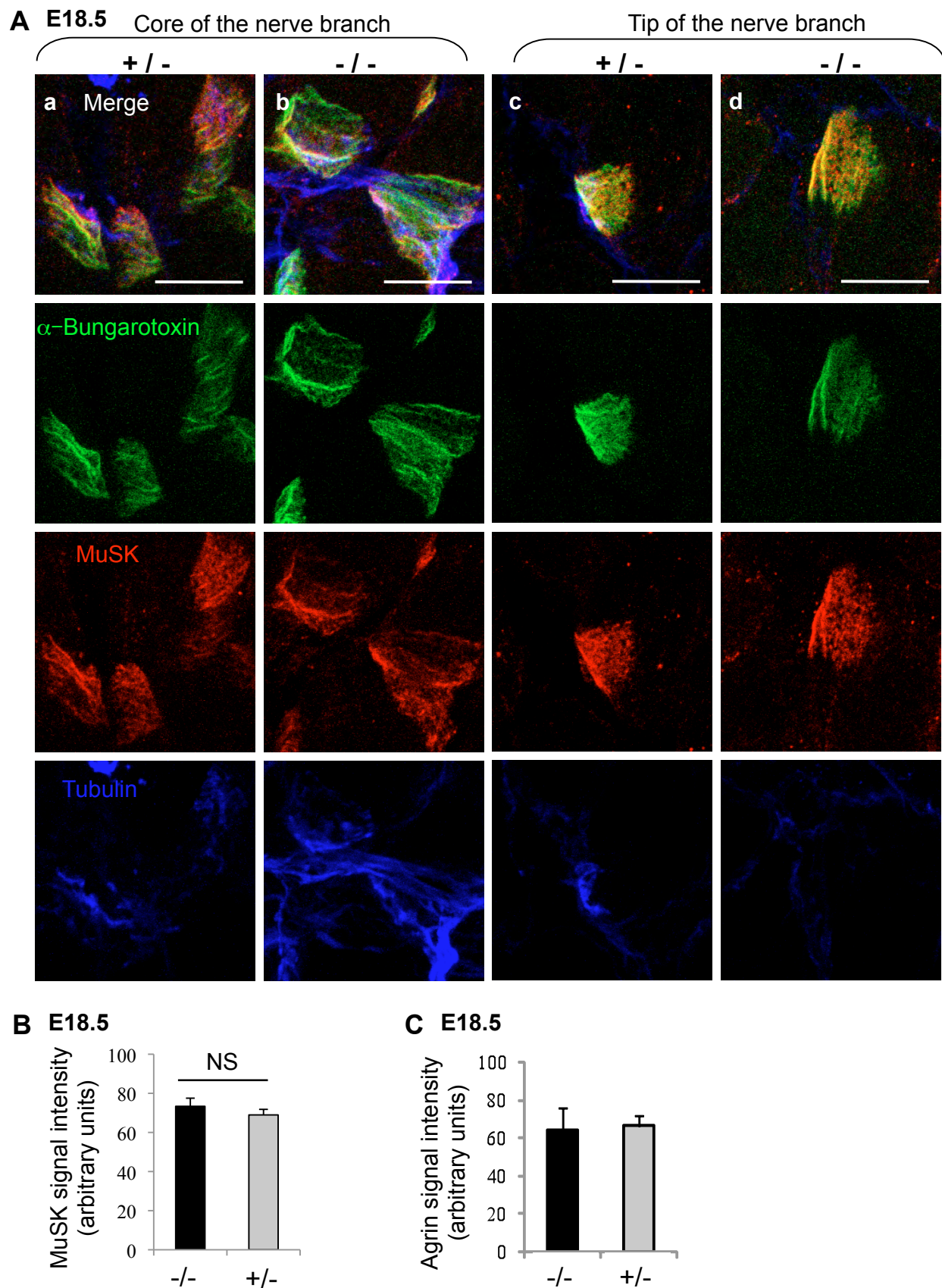
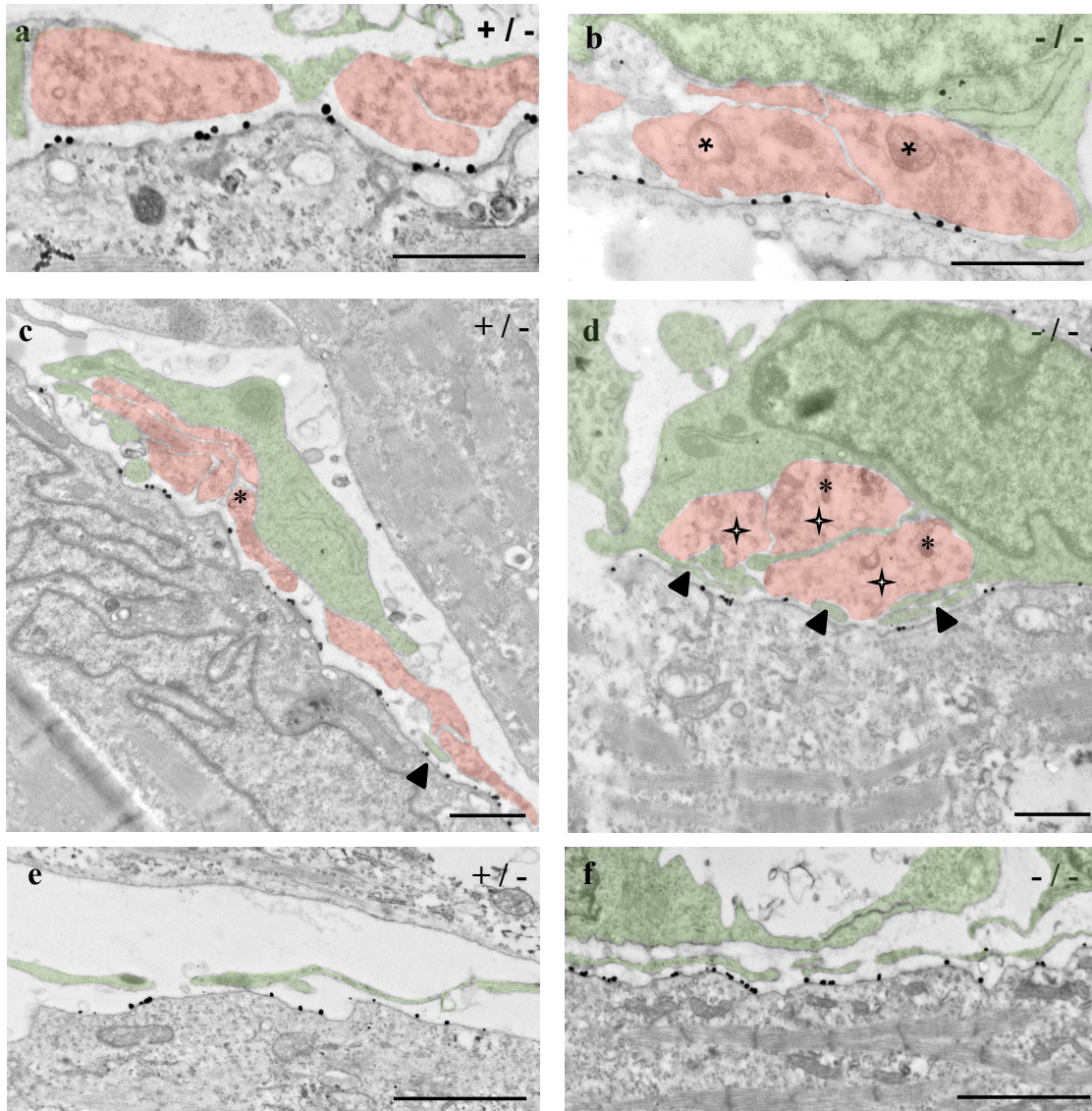


Fig. S4. Post-synaptic MuSK and neutrally secreted agrin are normally present at NMJs in E18.5 mutant diaphragms. Post-synaptic nAChRs and neuronal tubulin were labeled with α -bungarotoxin and Tuj1 antibody, respectively, and with either anti-MuSK or anti-agrin antibodies in diaphragm cryosections before imaging by confocal microscopy. (A) MuSK (in red) colocalized with nAChRs (in green) either at the core (a, b) or the tip (c, d) of the nerve ventral branch in both control and mutant diaphragms. (B,C) Measurement of (B) MuSK and (C) agrin fluorescent signal intensity at NMJs in the ventral part of E18.5 diaphragms. Data are mean \pm s.e.m. Mann-Whitney U test. NS, non-significant. Scale bar: 10 μ m.

A E15.5



B E15.5

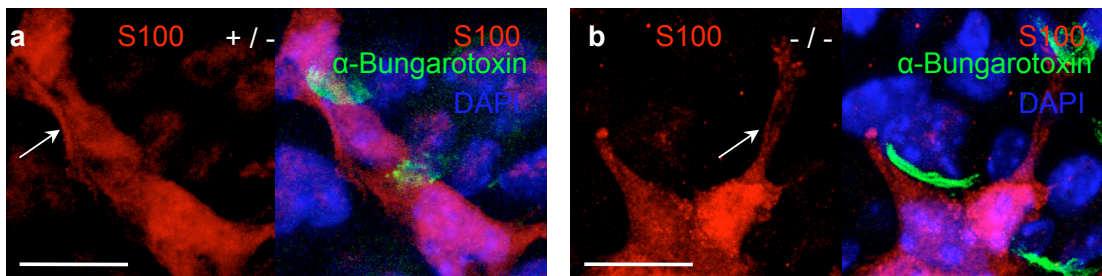


Fig. S5. At E15.5, some defects are already apparent at the ultrastructural level in few NMJs in the ventral part of mutant diaphragm muscle. (A) Longitudinal ultrathin sections were cut through muscle fibers of the ventral region of diaphragm of E15.5 embryos. NMJs were detected by labeling nAChRs with biotinylated α -bungarotoxin and streptavidin coupled to gold particles. Presynaptic nerve terminals and terminal Schwann cells are artificially colored in light red and green, respectively. In both control and mutant diaphragms, nerve terminals containing pre-synaptic vesicles and mitochondria (asterisks), and capped by large Schwann cells are observed at NMJ (a, b). However, in *Clipr-59* mutant, in some NMJs (stars in d) the nerve terminal composition appeared abnormal with few vesicles accumulating (but still some mitochondria, asterisks). The presence of Schwann cell processes in the synaptic cleft between presynaptic and post-synaptic components (arrowhead), and enwrapping nerve terminals could suggest their engulfment by Schwann cells. These Schwann digitations were observed to a lower extent in the synaptic cleft of some NMJs of control samples (c), and also in regions devoid of nerve terminals (d and e). (B) Using anti-S-100 antibody on E15.5 diaphragm cryosections, similar Schwann extensions were evidenced (arrow) by light microscopy in both control and mutant samples (a and b, respectively). Scale bars: 1 μ m in A; 10 μ m B.